# Independent innexin radiation shaped signaling in ctenophores

Jennifer Ortiz[1,2†], Yuriy V. Bobkov[1†], Melissa B. DeBiasse[1,3], Dorothy G Mitchell[1,4], Allison Edgar[1], Mark Q. Martindale[1,4], Anthony G. Moss[5], Leslie S. Babonis[1,6], Joseph F. Ryan[1,4,*]

[1] Whitney Laboratory for Marine Bioscience, University of Florida, St Augustine, FL 32080, USA

[2] Department of Biology, University of Washington, Seattle, WA 98105, USA

[3] School of Natural Sciences, University of California Merced, Merced CA 95343, USA

[4] Department of Biology, University of Florida, Gainesville, FL 32611, USA

[5] Biological Sciences Department, Auburn University, AL 36849, USA

[6] Department of Ecology and Evolutionary Biology, Cornell University, Ithaca, NY 14853, USA

[*] Corresponding Author: joseph.ryan@whitney.ufl.edu

†These authors contributed equally

**ABSTRACT:**

Innexins facilitate cell-cell communication by forming gap junctions or non-junctional hemichannels, which play important roles in metabolic, chemical, ionic, and electrical coupling. The lack of knowledge regarding the evolution and role of these channels in ctenophores (comb jellies), the likely sister group to the rest of animals, represents a substantial gap in our understanding of the evolution of intercellular communication in animals. Here we identify and phylogenetically characterize the complete set of innexins of four ctenophores: *Mnemiopsis leidyi*, *Hormiphora californensis, Pleurobrachia bachei*, and *Beroe ovata*. Our phylogenetic analyses suggest that ctenophore innexins diversified independently from those of other animals and were established early in the emergence of ctenophores. We identified a four-innexin genomic cluster, which was present in the last common ancestor of these four species and has been largely maintained in these lineages. Evidence from correlated spatial and temporal gene expression of the *M. leidyi* innexin cluster suggest that this cluster has been maintained due to constraints related to gene regulation. We describe basic electrophysiological properties of putative ctenophore hemichannels from muscle cells using intracellular recording techniques, showing substantial overlap with the properties of bilaterian innexin channels. Together, our results suggest that the last common ancestor of animals had gap junctional channels also capable of forming functional innexin hemichannels, and that innexin genes have independently evolved in major lineages throughout Metazoa.

## INTRODUCTION:

Ctenophores (comb jellies; Figure 1A) are marine animals defined by eight rows of ciliary paddles called comb rows. Ctenophores are capable of fast motor behaviors (e.g., ciliary reversal and tentacle retraction), have a number of neurosensory structures (e.g., nerve net, aboral organ, tentacles, sensory papillae), and possess a large suite of genes related to neural cell types and sensory information processing (Tamm 2014; Jager et al. 2011; Ryan et al. 2013). Nevertheless, ctenophore biology remains poorly understood, especially in relation to intercellular communication (Dunn et al. 2015). Genomic surveys in ctenophores looking for neurotransmitters and neurotransmitter pathways found in other animals have largely come up empty, and these results have formed the basis of the hypothesis that the ctenophore nervous system is a product of convergent evolution (Moroz et al. 2014). Phylogenomic evidence suggests that ctenophores are the sister to the rest of animals (Dunn et al. 2008; Figure 1B; Supplementary Table 1), and as such, are a key lineage for understanding the evolutionary history of animal nervous systems.

Gap junctions are assemblages of intercellular hemichannels that allow for the direct transfer of molecules and ions (up to ~1–3 kDa) between the cytoplasms of adjacent cells (Loewenstein 1966; Kanaporis et al. 2011; Oshima et al. 2013). In animals where gap junctions have been studied extensively, these channels have been detected joining virtually all cells in solid tissues (Goodenough and Paul, 2009). In the nervous system, gap junctions provide regulated pathways for the transfer of electrical signals (including bidirectional signaling), which often promote synchrony but can also

provide a range of other functionality including inhibition and shunting of excitatory potentials (Vaughn and Haas, 2022). Furthermore, growing evidence indicate that electrical synapses could also be subject to activity dependent long-term plasticity (O'Brien and Bloomfield, 2018; Welzel and Schuster, 2018; Alcamí and Pereda, 2019).

In vertebrates, gap junctions are formed by hemichannels consisting of six subunits of connexin proteins (Yeager and Harris, 2007). Vertebrates also have channels made of pannexin proteins (usually eight subunits), which unlike connexins, do not form gap junctions but instead are able to connect the cytoplasm of cells directly to the extracellular environment (Dahl and Locovei, 2006; Sosinsky et al. 2011). Connexin and pannexin channel proteins are very different at the sequence level and they are not thought to be homologous, but they share similarities at the level of membrane topology (Phelan et al. 1998; Yen et al. 2007).

Invertebrates lack connexins (Phelan et al. 1998), but they have innexins which belong to the same superfamily as the pannexin proteins (Yan et al. 2007). Unlike vertebrates where gap junction and functional hemichannel capabilities have been partitioned between connexins and pannexins, innexins can function as gap junctions or in their undocked form as non-junctional membrane channels called innexons (Dahl and Muller 2014; Linden et al. 2019). Thus, innexin proteins potentially mediate both electrical and nonelectrical/chemical communication pathways and are critical for many processes including embryonic development, reproduction, and neural function (Güiza et al. 2018).

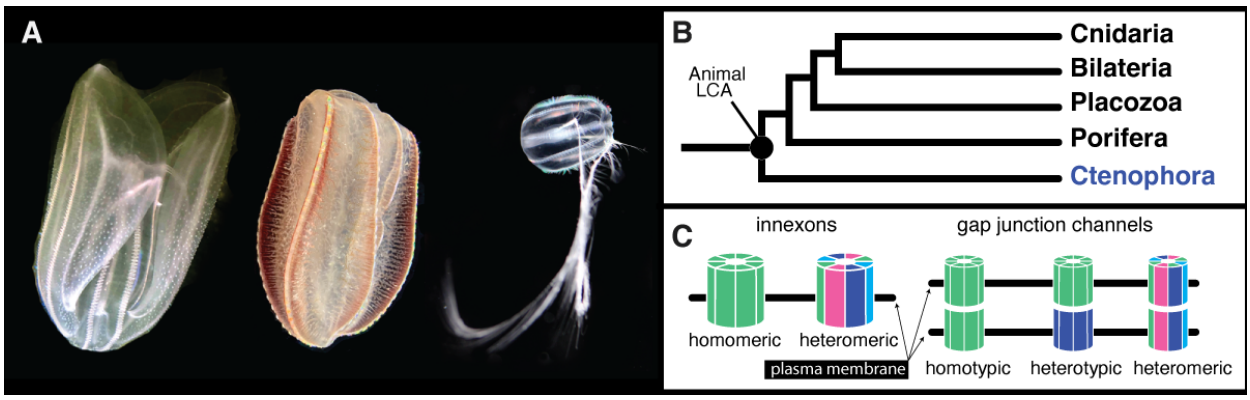


**Figure 1. Ctenophores and innexins.** (A) Three of the four ctenophore species in this study. From left to right: *Mnemiopsis leidyi*, *Beroe ovata*, and *Pleurobrachia bachei* (*Hormiphora californensis*, not pictured, is a tentaculate ctenophore with similar morphology to *Pleurobrachia*). (B) Based on phylogenomic evidence (Supplementary Table 1), Ctenophora is the sister group to the rest of animals. (C) Diagrammatic representation of potential subunit makeup of hemichannels and gap junctions (after Phelan and Starich 2001). Innexin subunits oligomerize to form a hemichannel. Hemichannels in adjacent cells can dock to form gap junctions. Hemichannels are either homomeric (composed of a single type of innexin) or heteromeric. Gap junctions are homotypic if hemichannels are identical, heterotypic if hemichannels are distinct, and heteromeric if hemichannels differ in subunit composition. *Mnemiopsis leidyi* photo by Arianna Rodriguez. Other photos by Joseph Ryan.

Gap junctional hemichannels are formed by connexin proteins (connexons) in vertebrates and innexin proteins (innexons) in both vertebrates and invertebrates. These two protein families are very different at the level of primary structure, but have similar topologies with four transmembrane domains (Bruzzone et al. 1996; Phelan and Starich 2001). The number of subunits per gap junctional hemichannel is variable (Oshima et al. 2016). In addition, subunit composition of gap junctional hemichannels can be homomeric (composed of a single innexin type) or heteromeric (composed of

multiple innexin types). Likewise, gap junctions can be homotypic (composed of two homomeric hemichannels), heterotypic (composed of two different homomeric hemichannels), or heteromeric (composed of two heteromeric hemichannels; Figure 1C; Koval et al. 2014; Hall 2017).

Innexins are specific to animals. They are widely distributed throughout animals (Yen and Saier 2007) including ctenophores (Ryan et al. 2013; Moroz and Kohn, 2016; Slivko-Koltchik et al. 2019; Welzel and Schuster, 2022), but have not yet been identified in the genomes of sponges (Leys 2015), placozoans (Senatore et al. 2017), echinoderms (Slivko-Koltchik et al. 2019), hemichordates (Welzel and and Schuster, 2022), anthozoan cnidarians (Satterlie, 2015), and scyphozoan cnidarians (Satterlie, 2015). Phylogenetic analyses of innexins show a striking pattern of lineage-specific radiations throughout animal history (Yen and Saier 2007). Consistent with this finding, a subset of innexins from the ctenophore *Pleurobrachia bachei* were analyzed phylogenetically and shown to be more closely related to each other than to non-ctenophore innexins (Slivko-Koltchik et al. 2016). Another study identified a number of innexins in a range of ctenophore species, but none of these were complete sets from sequenced genomes and trees that included these sequences were not reported in the study (Welzel and Schuster, 2022). As such, the lack of a comprehensive phylogenetic analysis that incorporates complete genomic data from multiple ctenophore species represents a substantial gap in our understanding of innexin evolution.

While electrophysiological properties of gap junction and/or innexin hemichannels in ctenophores are unknown, high similarity of functional domains of ctenophore innexins and their relatively well studied bilaterian counterparts suggests

similar physiological properties. Several basic properties of bilaterian gap junctions have been established. For example, it is known that innexin channels are nonselective, exhibit high conductance and sometimes multiple subconductance states, and are activated by intracellular calcium at physiologically relevant concentration ranges (Locovei et al. 2006; Dahl and Muller 2014).

Ultrastructural studies have offered a partial map of the anatomical distribution of gap junctions and therefore have provided insights into the functions of gap junctions in ctenophores. In *Pleurobrachia bachei*, gap junctions connect individual cilia within a comb plate (paddle-shaped bundles of thousands of cilia that comprise a comb row) suggesting a role in coordinating activity within individual plates (Satterlie and Case 1978). Satterlie and Case (1978) also observed gap junctions in the meridional canals (endoderm) that underlie the comb rows of *P. bachei*. Anctil (1985) later showed that the light-producing photocytes within the meridional canals of *Mnemiopsis leidyi* are linked to each other via gap junctions suggesting a possible role in the coordination of conduction of flashes along these canals. There is also ultrastructural evidence of gap junctions between muscle cells in *Beroe ovata* (Hernandez-Nicaise and Amsellem 1980) and *Mnemiopsis leidyi* (Hernandez-Nicaise et al. 1984). Together these data suggest that gap junctions play a key role in intercellular communication between a wide array of ctenophore cell types including neurons, photocytes, and muscle cells, and likely play a role in electrical synapses in ctenophores (Horridge 1974; Satterlie and Case 1978; Tamm 1982; Tamm 1984; Hernandez-Nicaise et al. 1989).

The current understanding of gap junctions in ctenophores is limited to ultrastructural studies and to phylogenetic analyses of a subset of innexins in a single

155 species. Here, we phylogenetically annotate the innexins of four species of
156 ctenophores, establish the classification and nomenclature of ctenophore innexins,
157 show a conserved genomic architecture associated with innexin gene regulation and
158 genomic evolution, conduct whole-mount in situ hybridization to observe the spatial
159 expression of the four genomically clustered innexins in *Mnemiopsis*, use transcriptomic
160 evidence to associate innexin families with specific cell types, and provide
161 electrophysiological evidence of innexin activity. The work provides a high resolution
162 view of the evolution of innexins in ctenophores and has implications for the evolution of
163 animal neuromuscular systems.
164
165 **MATERIALS AND METHODS:**
166
167 ***Transparency and Reproducibility***
168
169 Prior to conducting all phylogenetic analyses, we constructed and published a
170 phylotocol (DeBiasse and Ryan 2019) on GitHub that outlined our planned analyses.
171 Any adjustments to the phylotocol during the course of the study have been outlined
172 and justified in the current version of the phylotocol. These adjustments are available
173 along with alignments, trees, and commands used in this study at:
174 https://github.com/josephryan/ctenophore_innexins (referred to as the project GitHub
175 repo throughout; repo snapshot available as Supplemental File 1).
176
177 ***Identification of ctenophore innexins***

178

179 To identify innexins in the ctenophore species *Beroe ovata*, *Mnemiopsis leidyi*,
180 *Pleurobrachia bachei*, and *Hormiphora californensis*, we BLASTed the corresponding
181 ctenophore protein models with Inx2 from *Drosophila melanogaster* (GenBank
182 accession=NP_001162684.1). Any ctenophore sequence that BLASTed back to a *D.*
183 *melanogaster* innexin was considered for downstream analyses. This query sequence
184 was selected because of its relatively limited genetic change relative to other bilaterian
185 innexins as evident from its short branch length in a recent phylogenetic study (Table
186 SX of Abascal and Zardoya 2012). We used BLASTP with default settings and E-value
187 cutoff of 1e-3 to search against protein models from *M. leidyi*, *P. bachei*, *H.*
188 *californensis*, and B*. ovata*. The *B. ovata* innexins were recovered from an unpublished
189 genome assembly. We also analyzed a transcriptomic dataset of *H. californensis* (prior
190 to the publication of the *H. californensis* genome). We used TBLASTN rather than
191 BLASTP for the transcriptomic dataset with the same E-value cutoff (1e-3). As
192 transcriptome assemblies often contain multiple isoforms for a single gene (sometimes
193 but not always labeled as isoforms), we generated a preliminary maximum-likelihood
194 tree with IQ-TREE using default parameters and removed *H. californensis* innexin
195 transcripts that had zero-length branches relative to another sister *H. californensis*
196 innexin transcript.

197

198 ***Phylogeny***

199

We aligned each putative innexin that we identified to the Innexin PFAM domain (PF00876) and removed any sequence flanking the domain. We then aligned these sequences with MAFFT v.7.407 (Katoh and Toh 2008) using default parameters. We used this alignment to generate a maximum-likelihood tree with IQ-TREE with default parameters. We also used RAxML v.8.2.11 to generate a maximum-likelihood tree, choosing the tree with the highest likelihood value from 50 runs including 25 with starting parsimony trees and 25 with random starting trees. Lastly, we generated a Bayesian tree using MrBayes v3.26 (Ronquist and Huelsenbeck 2003). We used RAxML to generate likelihood scores for the IQ-TREE and MrBayes phylogenies and compared all four of these independent analyses, choosing the one with the highest likelihood value as our main tree. Our justification for applying multiple likelihood methodologies with multiple starting trees is that empirical analyses have shown that performance of likelihood methods and parameters are variable between datasets (Zhou et al. 2018).

The publication of the *H. californensis* genome followed the completion of our initial extensive phylogenetic analysis. To incorporate these new data into this study, we conducted a more streamlined phylogenetic analysis. As in our original analysis we aligned each putative innexin to the Innexin PFAM domain and removed flanking sequences. In cases where there were more than 1 isoform, we kept one representative based on maximizing the number of residues recognized by the PFAM domain search. Unlike in the original analysis, we did not align with MAFFT, instead we removed insertions from the alignment generated by the hmmsearch tool (with -A parameter) from HMMer (Finn et al. 2011). This approach greatly sped up the process

and did not change the results of reanalyzed datasets. In this analysis we expanded the outgroups to include all the innexins from the genomes of the following species: *Branchiostoma lanceolatum* (Chordata), *Capitella teleta* (Annelida), *Lottia gigantea* (Mollusca), *Nematostella vectensis* (Cnidaria), and *Schistosoma mansoni* (Platyhelminthes). These additional sequences were all downloaded from release 51 of Ensembl Metazoa (Kinsella et al. 2011). We generated a maximum-likelihood tree from the resulting alignment using RAxML v.8.2.12 with the LG model.

### *Beroe ovata genomic data*

The *B. ovata* contig that contains INXB–D is from a preliminary assembly of the *B. ovata* genome and has been uploaded to the GitHub repository associated with this study. We have made the latest *B. ovata* genome assembly available at BovaDB (http://ryanlab.whitney.ufl.edu/bovadb). In addition, the *B. ovata* gene models for each of the innexins have been uploaded to this GitHub repository as well.

### *Single-cell/embryo Innexin RNA expression*

We used the *Mnemiopsis* Genome Project Portal (Moreland et al. 2020) to gather temporal expression information for each *M. leidyi* innexin. These temporal expression profiles were based on single-embryo developmental expression data reported in Levin et al. (2016) and Hernandez and Ryan (2018). We report the occurrence of *M. leidyi* innexins in expression clusters (approximate cell types) from

adult single cell RNA-Seq data (Sebe-Pedros et al. 2018). We created a Perl script (print_coexp_all.pl in the project GitHub repo) to parse unique molecular identifier (UMI) counts from supplemental files of Sebe-Pedros et al. (2018) and count co-expression of innexins in individual cells based on these data.

***Animal culture for whole-mount in situ hybridization***

*Mnemiopsis leidyi* adults were collected from floating docks in marinas surrounding the St. Augustine FL, USA area. Wild-caught animals spawned overnight in accordance with their circadian rhythm (Sasson and Ryan 2016) and their embryos were collected and reared to cydippid stages in filtered natural seawater. Cydippids were fed rotifers (*Brachionus plicatilis*, L-type, Reed Mariculture, Campbell, CA) ad libitum until they reached spawning size (~0.5-2 mm diameter). Prior to fixation, animals were starved for at least 24 hours in UV-sterilized, 1 µm-filtered natural sea water.

***RNA probe design and synthesis for whole-mount in situ hybridization***

Probe templates were synthesized in vitro (by GenScript) based on known full-length coding sequences (1-1.2 kb) for each of the four target *M. leidyi* innexin genes. Probe sequences were checked against one another using Clustal Omega and with BLAST searches against the whole *M. leidyi* genome (Ryan et al. 2013) to ensure low likelihood of nonspecific binding. Digoxigenin-labeled antisense RNA probes were

268 synthesized using the Ambion MEGAscript Kit (AM1334). Probe sequences are
269 provided in Supplementary Table 2.
270
271 ***Fixation and whole-mount in situ hybridization***
272
273 Cydippids were fixed following Mitchell et al. (2021). Briefly, animals were fixed
274 in 16% Rain-X Original Formula for 1 hour at room temperature and subsequently post-
275 fixed with ctenophore in situ fixation buffer 1 (4% paraformaldehyde + 0.02%
276 glutaraldehyde in FSW) for 5 minutes and ctenophore fixation buffer 2 (4%
277 paraformaldehyde in FSW) for 1 h at room temperature in flat-bottomed, 24-well
278 polystyrene plates. Fixed samples were dehydrated into methanol and then stored in
279 100% methanol at -20°C for at least 16 hours. Whole-mount in situ hybridization was
280 performed following Pang and Martindale (2008), with detection being modified slightly
281 using a 4:1 ratio of nitro-blue tetrazolium chloride: 5-bromo- 4-chloro-3-
282 indolylphosphate toluidine salt. Each of the four probes were developed for at least 24
283 hours with the no probe control being developed as long as the slowest probe and
284 washed with 50mM EDTA to stop the reaction. Samples were then washed several
285 times with PTw (PBS + 0.1% (v/v) Tween-20) and then cleared in 80% glycerol at 4°C
286 for several days. Cleared samples were imaged on a Zeiss AxioImager M2 microscope.
287
288 ***Tissue RNA*-Seq**
289

We leveraged previously published tissue-specific RNA-Seq data from *M. leidyi* tentacle bulbs and comb rows that were reported in Babonis et al. (2018). To this we added transcriptome data from *M. leidyi* aboral organs that were collected and sequenced in the same way (all with 3 replicates) and at the same time as the other tissue data. We dipped medium-sized (20-35mm) *M. leidyi* adult individuals from floating docks in marinas surrounding the St. Augustine FL, USA area. Aboral organs were carefully excised and were snap-frozen using dry ice. RNA extraction, library preparation, and sequencing were performed by the Interdisciplinary Center for Biotechnology Research at the University of Florida. Three independent replicates, each of a single extraction from a single individual, were sequenced on a single lane of a HiSeq 3000 using a paired-end protocol. Raw sequence data have been deposited in the European Nucleotide Archive (accession PRJNA787267).

We used the rsem-calculate-expression script from RSEM version 1.3.0 (Li and Dewey, 2011) with the --bowtie2 option to align reads to the ML2.2. gene models. We used DESeq2 v1.20.0 (Love et al. 2014) to generate normalized counts in the form of transcripts per million (TPM) from these alignments.

***Electrophysiology and data analysis***

We performed whole-cell voltage clamp recordings to detect and characterize the activity of putative gap junction channels in isolated *M. leidyi* muscle cells. To isolate muscle cells, we dissected small sections from adult ctenophore lobes containing muscle and mesoglea (extracellular matrix). Samples (from 15 individuals in

313 total) were triturated with micropipette in 400-500 µL modified artificial sea water
314 (extracellular solution: 486 mM NaCl, 5 mM KCl, 13.6 mM $CaCl_2$, 9.8 mM MgCl2, 10
315 mM HEPES, and pH adjusted to 7.8 with NaOH or Tris-base) to separate individual
316 cells. Dissociated cells were then plated on 35-mm Petri dishes filled with artificial sea
317 water and allowed to settle for at least one hour before recording. We used Axiovert
318 100 (Carl Zeiss Inc., Germany) or Olympus IX-71 (Olympus Corp., Japan) inverted
319 microscopes to visualize cells. Smooth muscle cells were identified morphologically by
320 their elongated shape and numerous processes and by their ability to contract either
321 spontaneously or after being stimulated with glutamate (Supplementary Movie 1) or
322 high potassium solution. Intracellular solution used in whole cell recordings contained
323 (in mM): 210 mM KCl, 696 mM Glucose, 0 mM $Ca^{2+}$, 1mM EGTA, 10mM HEPES, with
324 NaOH or Tris-base to adjust pH to 7.8 (intracellular low calcium solution) or 210 mM
325 KCl, 696 mM Glucose, 0 mM EGTA, 0.001 mM $CaCl_2$, 10 mM HEPES, and NaOH or
326 Tris-base to adjust pH to 7.8 (intracellular high calcium solution). Calcium concentration
327 in intracellular high calcium solution was likely higher than 1µM.

328 We pulled patch electrodes from borosilicate capillary glass (BF150-86-10,
329 Sutter Instruments, USA) using a Flaming-Brown micropipette puller (P-87, Sutter
330 Instruments, USA). Resistance of the electrodes was 1–3 MΩ as measured in artificial
331 sea water. Currents were measured with either an Axopatch 200A or 200B patch-clamp
332 amplifier (Molecular Devices, USA) using an AD–DA converter (Digidata 1320A,
333 Molecular devices, USA), low-pass filtered at 5 kHz, and sampled at 5–20 kHz. Data
334 were collected and analyzed with pCLAMP 9.2-10 software (Molecular Devices, USA)
335 in combination with SigmaPlot 10-14 (SPSS, USA). Only cells characterized by a cell-

attached patch seal resistance ≥1 GΩ and a relatively high input resistance (≥300 MΩ, 1.1±0.3 GΩ on average) were chosen for analysis. After establishing the whole-cell voltage clamp mode, we monitored the activity of currents at a holding potential of -60 to -70 mV for 2–5 minutes. Then the muscle cells were initially hyperpolarized by -40 to -50 mV and 200 ms voltage steps were applied in 10 mV increments. All current traces free from the activity of voltage-gated channels, typically in the range -120-(-40) mV, were carefully reviewed on possible high conductance channel activity. We performed all recordings at room temperature.

We used single channel currents to generate current-voltage relationships. The reversal potential estimates based on single channel currents are more accurate since the direct measurement of unitary currents eliminates or reduces the necessity for pharmacological dissection of integral currents (Bobkov et al., 2011). The reversal potential estimates for potassium ($V_r$,$K^+$), chloride ($V_r$,$Cl^-$) and monovalent cation ($V_r$,$X^+$) selective channels were calculated using Nernst equation.

## RESULTS

### *Innexins in ctenophores*

We identified 9 innexins in *Pleurobrachia bachei,* 19 in *Hormiphora californensis,* and 12 in both *Mnemiopsis leidyi* and *Beroe ovata.* We performed a range of maximum-likelihood and Bayesian analyses to phylogenetically classify these innexins. We found

359 that all ctenophore innexins are most closely related to other ctenophore innexins
360 (Figure 2A) and have therefore radiated in parallel to the innexins of other animals
361 (Figure 2B). The ctenophore innexins have substantial conservation in the four regions
362 predicted to be the transmembrane helices, contain the four highly conserved
363 extracellular cysteines, and include the conserved proline in the second
364 transmembrane domain (Supplementary Figure 1).

365 Based on our phylogeny, we identified 17 ctenophore innexin families that we
366 have named INXA–INXR (we did not include an INXI to avoid confusion with INX1 in
367 other species; Figure 2A). To infer gene gains/losses (Figure 2B), we assumed that
368 absence from a clade indicates a historical gene loss and multiple genes from the same
369 species in a single clade indicates a historical gene duplication (parsimony principles).
370 We infer that 14 innexin families (i.e., INXA–D,G,H,J–O,Q,R) arose in the stem
371 ancestor of Ctenophora, INXP arose in the last common ancestor of *B. ovata* and *M.*
372 *leidyi*, INXE arose in the last common ancestor of *P. bachei* and *H. californensis*, and
373 INXF arose in the *H. californensis* lineage. We inferred 13 gene losses within these
374 ctenophore lineages including four in the *M. leidyi* lineage (INXK, N, Q, and R), two in
375 the *B. ovata* lineage (INXA and J), seven in the lineage leading to *P. bachei* (INXA, G,
376 H, K, O, Q, and R) and none in the lineage leading to *H. californensis*. We identified
377 four duplications including one in the lineage leading to *P. bachei* and *H. californensis*,
378 one in the *M. leidyi* lineage (INXG), and two in the *H. californensis* lineage (INXJ and
379 F). Names and accessions of ctenophore innexins are provided in Supplementary
380 Table 3.
381

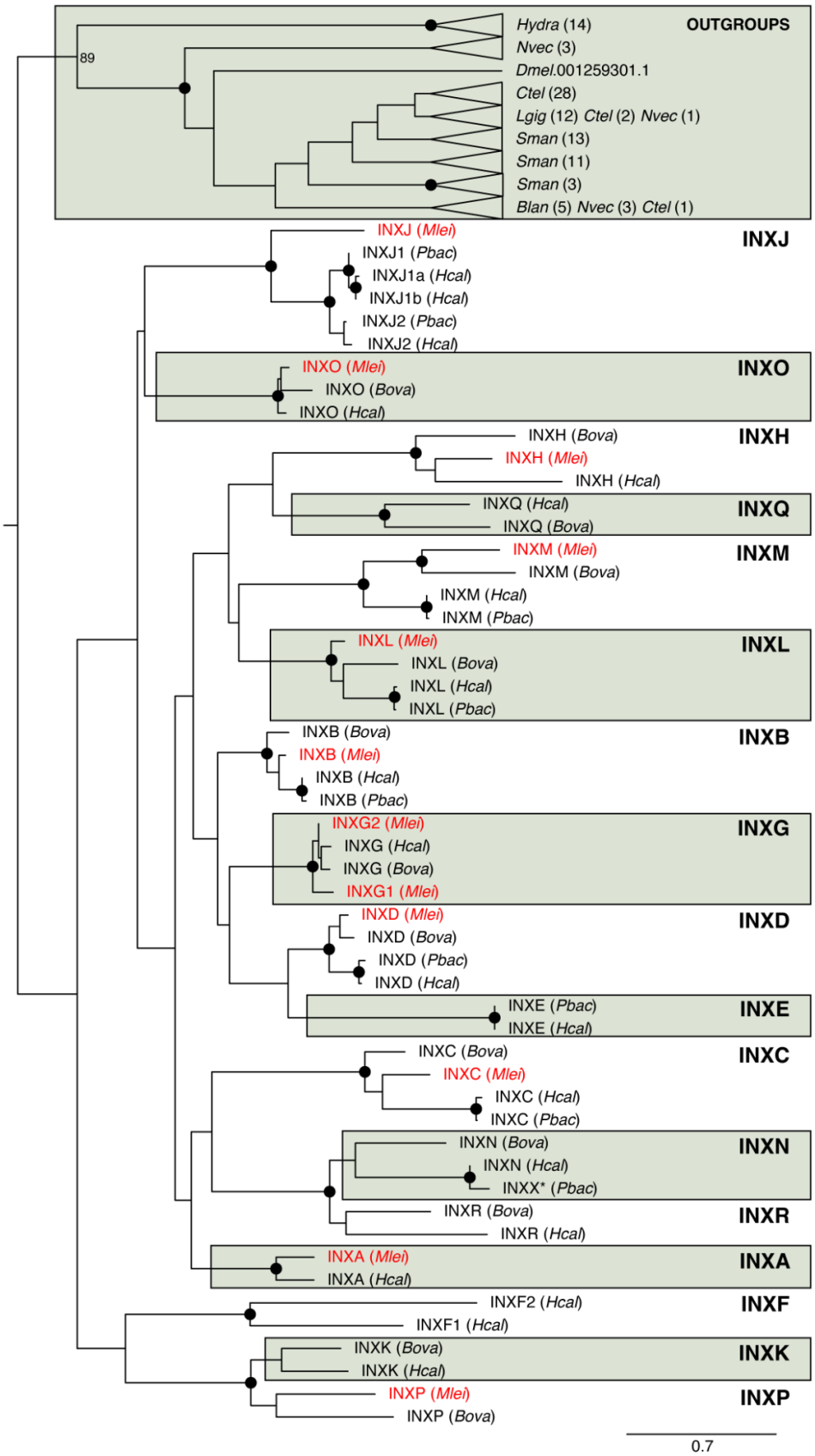

**Figure 2. Evolution of ctenophore innexins.** (A) Maximum likelihood tree of innexins from four ctenophore species *Mnemiopsis leidyi* (Ml), *Pleurobrachia bachei* (Pb), *Beroe ovata* (Bo), and *Hormiphora californensis* (Hc) as well as full sets of innexins from non-ctenophores including *Hydra vulgaris* (Cnidaria), *Nematostella vectensis* (Cnidaria), *Capitella teleta* (Annelida), *Lottia gigantea* (Mollusca), *Schistosoma mansoni* (Platyhelminthes), *Branchiostoma lanceolatum* (Chordata), as well as Inx2 from *Drosophila melanogaster* (Arthropoda). Solid circles at the nodes indicate bootstrap support greater than or equal to 90%. A version of this tree with all bootstrap values and without collapsed outgroup clades is available as Supplementary Figure 2.

### *Conserved genomic cluster of Innexins*

The INXB, INXC, and INXD genes are within 40 kilobases of each other in each of the *M. leidyi*, *P. bachei*, and *B. ovata* genomes (Figure 3A). These clusters include no detectable intervening non-innexin genes. In *M. leidyi*, a fourth innexin, INXA, is less than 40 Kb upstream of the INXB-D cluster. Between INXA and INXB are three non-innexins, an ankyrin-related gene (ML25994a), an undescribed ctenophore specific gene (ML25995a), and an intraflagellar transport-related gene (ML25996a). The *B. ovata* INXB-D cluster spans 33 Kb. INXA was not recovered in *B. ovata* or *P. bachei*.

INXB, INXC, and INXD are adjacent on chromosome 10 of the chromosome-level assembly of the recently sequenced genome of *Hormiphora californensis* (Schultz et al. 2021). There are 226 genes between INXA and the INXB-D cluster in *H. californensis*. Microsynteny is rare between *H. californensis* and *M. leidyi* with the largest identifiable blocks of gene microsynteny including only four genes (Schultz et al.

2021), but the block that includes INXB, INXC, and INXD is conserved and also includes a fourth gene (ML259910a in *M. leidyi* and Hcv1.av93.c10.g249.i1 in *H. californensis*), which is similar to the FAM166B gene in humans. Interestingly, INXN (Hcv1.av93.c10.g18.i1), which was lost in *M. leidyi*, is next to INXA in *H. californensis* and INXG (Hcv1.av93.c10.g192.i1) is situated in between these two sets of innexins (173 genes downstream from INXA and 54 genes upstream of INXB) suggesting the cluster was once more extensive.

### *Innexin gene expression*

We compared the gene expression profiles of *M. leidyi* innexins during early development, in adult tissues, and in adult single cells. In all of these data, INXB and INXD expression levels are orders of magnitude higher than all other innexins (Figure 3B). Our single-embryo RNA-Seq time-course data (Levin et al. 2016; Hernandez and Ryan 2018) show that INXB and INXD have highly coordinated expression patterns throughout development (Figure 3B).

We identified evidence of innexin co-expression in the single-cell RNA-Seq data in *M. leidyi* from Sebé-Pedrós et al. (2018). In this study, the gene expression profiles of individual cells from a dissociated adult animal were clustered to construct metacells, which approximate cell types. Any gene expressed in at least 50% of the cells comprising a metacell were considered marker genes. INXB and INXD were considered co-marker genes in a digestive (C3), 'smooth' muscle (C44), and 3 epithelial metacells (C14,15,17; Figure 3D). INXO and INXG1 were considered marker genes in two neural

metacells (C33,34) INXH and INXL, were considered marker genes for two comb plate metacells (C48,49; Figure 3D; Supplementary Table 4).

Beyond metacells, we analyzed innexin expression in individual cells using the UMI data from the supplemental data of Sebé-Pedrós et al. (2018). The majority of the cells in this dataset express at least one innexin (63%), 34% of cells express at least two innexins, and one cell expresses 9 innexins (Figure 3C; Supplementary Table 5). These numbers are likely an underestimate as the depth of sequencing in this study (average of 36,000 reads per cell and 5 reads per UMI) was low compared to more recent single-cell RNA-Seq studies. We identified 10 instances where 50% of the cells expressing a specific innexin also expressed another innexin. Most of these pairings involve the highly expressed INXB and INXD genes including: INXB-INXC, INXB-INXG2, INXB-INXP, INXB-INXJ, INXD-INXJ, INXD-INXC, but several pairings did not include INXB and INXD including: INXG1-INXG2, INXH-INXA, INXH-INXL, INXH-INXM (Figure 3E; Supplementary Table 6).

Like the developmental time course data, the single-cell RNA-Seq data lend support to the hypothesis that the innexin genome cluster (Figure 3A) has a role in coordinating expression of INXA–D. For example, INXB is expressed in 1,761 (70%) of the cells that express INXD (Figure 3E; Supplementary Table 6). In addition, INXB and INXD are expressed in 53.5% of cells expressing INXC and in 37.8% of cells expressing INXA (Supplementary Table 6). It is important to note that while INXC is not a defining gene for any metacells (likely due to more moderate levels of expression compared to INXB and INXD) and therefore lacks any shaded cells in Figure 3D, it is expressed widely (Figure 4F).

We next identified co-expression of *M. leidyi* innexins in tissue-specific RNA-Seq data from tentacle bulbs and comb rows (Babonis et al 2018) as well as aboral organs (this study; principal components analysis in Supplementary Figure 3). As in our other expression data, INXB and INXD are both highly expressed relative to other innexins and are expressed at similar relative levels in each tissue (i.e. both are expressed higher in aboral organ tissue than in tentacle bulbs and lowest in comb rows; Figure 3 F–G). The tissue RNA-Seq expression patterns also bolster evidence for other innexins that might be working together in either a heteromeric or heterotypic capacity. For example, INXL and INXH, which were implicated in the single-cell RNA-Seq data as being involved in comb plate cells, are expressed at relatively high levels in comb row tissues and at very low levels or not at all in aboral organ and tentacle bulb samples (Figure 3G).

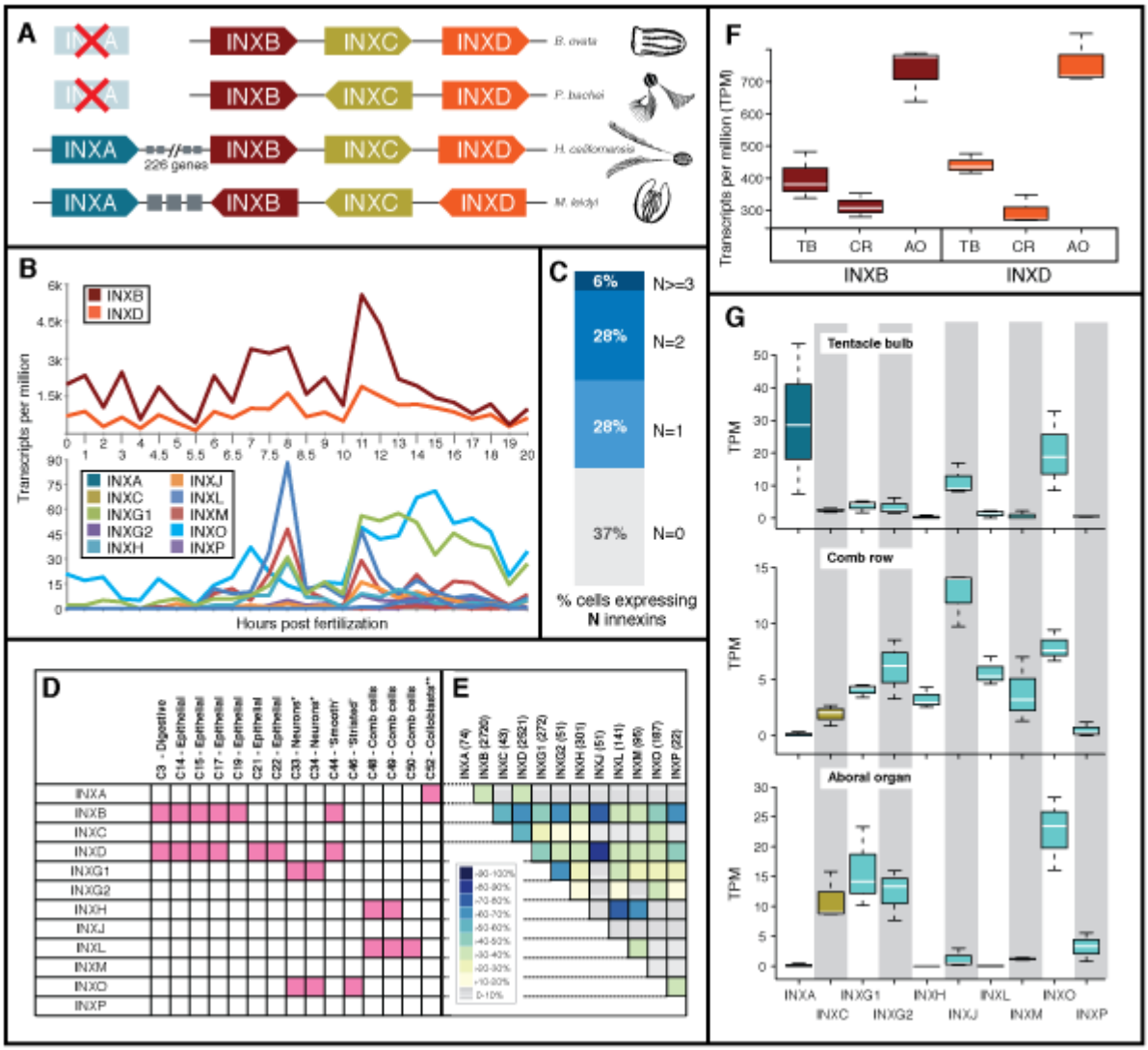


**Figure 3: temporal, cellular, and spatial expression of Innexins**. (A) Innexin clusters in the genomes of *Beroe ovata*, *Pleurobrachia bachei*, *Hormiphora californensis*, and *Mnemiopsis leidyi*. *Mnemiopsis leidyi* has a four-gene Innexin cluster that includes INXA, INXB, INXC, and INXD. The genomes of *B. ovata* and *P. bachei* have a cluster that includes INXB, INXC, and INXD. Grey boxes represent 3 non-innexin genes between INXA and INXB in *M. leidyi*. All four of these innexins are on chromosome 10 in *H. californensis*, but there are 226 genes separating INXA and INXB. The clusters are not to scale. In all genomes INXB, INXC, and INXD are within 20Kb of each other and in *M.leidyi*, the entire cluster including INXA is less than 80Kb. (B) Temporal gene expression in single *M. leidyi* embryos during the first 20 hours

of development (Levin et al. 2016) shows that INXB and INXD are both highly expressed and are tightly coordinated (top section). Comb plates are formed at 8 hours post fertilization and at this point there is a spike in expression of several innexin genes that are expressed in comb-plate cell types and tissues (i.e., INXL, INXM, INXG.1, INXH, INXJ, and INXP). (C) Percentage of single cells expressing 0, 1, 2, or >3 innexins (Supplementary Table 4). (D) Columns represent metacells from single-cell data (Sebe-Pedros et al. 2018). Pink squares represent expression of the corresponding innexin in 50% or more of the cells that make up the specified metacell (full counts per metacell are in Supplementary Table 5). (E) Heatmap of co-expression of each innexin in individual cells. The number of individual cells that express each innexin are in parentheses (in the column header). The percentage was determined by taking the number of cells with co-expression divided by the lowest number when comparing the number of individual cells that express each innexin (full co-expression counts are in Supplementary Table 6). (F) Expression of *M. leidyi* INXB and INXD in three replicates of bulk tissue RNA-Seq from tentacle bulbs (TB), comb rows (CR), and aboral organ (AO). INXB and INXD are shown separately because they are very highly expressed relative to the other innexins. (G) Expression of *M. leidyi* innexins in three replicates of bulk tissue RNA-Seq from tentacle bulbs, comb rows, and aboral organ. * Metacells C33 and C34 were hypothesized to be neurons in Sachkova et al. (2021). ** Metacells C52 were hypothesized to be colloblasts in Babonis et al. (2018).

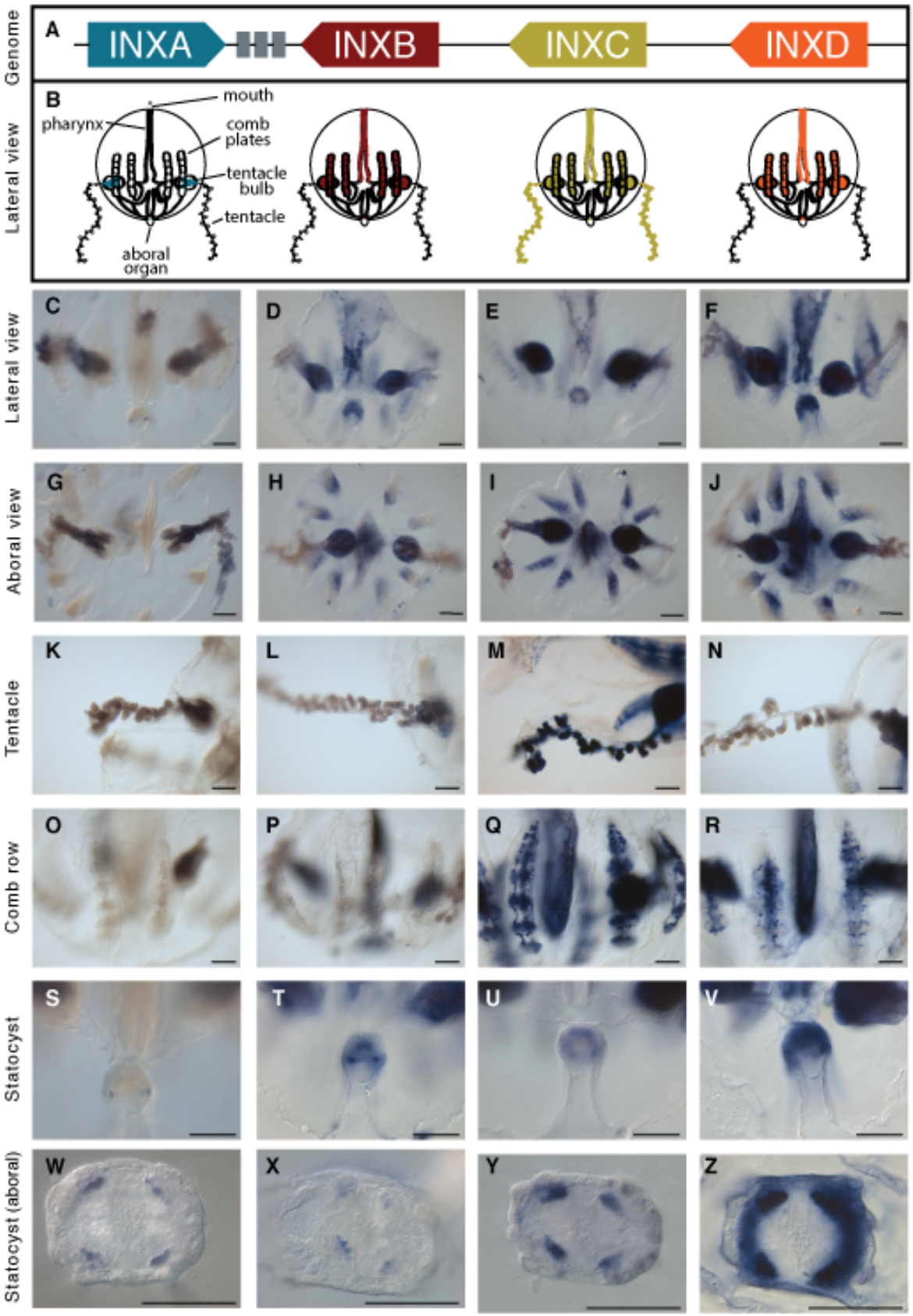

**Figure 4. Whole-mount in situ hybridization for four clustered *Mnemiopsis leidyi* innexin genes.** (A) Cartoon depiction of the innexin genomic cluster. (B) Cartoon representation of spatial patterns of expression of INXA-D. Specific patterns within expression domains of INXB-D are not shown due to slight variations in patterns between individuals. Seemingly overlapping domains in cartoons may not indicate co-expression in the same cells. (C-Z) In situ expression of INXA-D. The label to the left of each row describes the view or tissue under focus. Columns correspond to positions of genes in the genomic cluster of panel A. (C,G,K) INXA is highly expressed in the lateral ridge of the tentacle bulb. (O) INXA is not expressed in the comb rows or underlying canals. (S,W) There are four distinct INXA domains of expression in the aboral organ. (D,H) INXB is widely expressed in the tentacle bulbs,pharynx, aboral organ, and meridional canals underlying the longitudinal comb rows. (L) INXB is expressed in the tentacle bulb, but not the tentacle. (P) There is punctate INXB expression in the meridional canals underlying the comb rows. (T,X) There are four distinct INXA domains of expression in the aboral organ. (E,I) INXC is widely expressed in the tentacle bulbs, comb rows, pharynx, and aboral organ. (M) INXC has a distinct expression domain in the tentacles. (Q) INXC is expressed in the comb rows and in the underlying meridional canals. (U, Y) There are four distinct INXA domains of expression in the aboral organ. (F, J) INXD is widely expressed in the tentacle bulbs, comb rows, pharynx, and aboral organ. (N) INXD is not expressed in the tentacles. (R) There is punctate INXD expression in the meridional canals underlying the comb rows. (V, Z) INXD is expressed in a ring in the aboral organ. Coloration in the tentacles of INXA, INXB, and INXD is likely background. No probe controls are in Supplementary Figures 4–5. Patterns are representative of replicates (Supplementary Figures 6–9). All scale bars represent 100 μm.

522 ***Spatial expression of clustered innexin genes***

523

524 We examined the localization of mRNA expression of INXA–D by whole-mount
525 in situ hybridization in cydippid-stage *Mnemiopsis leidyi* (Figure 4). INXA expression,
526 which is present only in one of the colloblast cell types in the single-cell data and is
527 highest in the tentacle bulbs in our tissue RNA-Seq, is present almost exclusively in the
528 tentacle bulbs in our in situ expression analyses. In particular, the expression is
529 localized to the lateral ridge of the tentacle bulb and the tentacle root (Figure 4G, 4K).
530 This expression domain in combination with the single-cell data is consistent with INXA
531 being expressed in developing colloblasts. INXC on the other hand is expressed in a
532 wider domain in the tentacle bulbs (Figure 4E, 4I) and is also clearly expressed in the
533 tentacles themselves (Figure 4M). INXC is not expressed in colloblasts in the single cell
534 data, but is most highly expressed in single cells hypothesized to be neurons by
535 Sachkova et al. (2021; Supplementary Table 5). Together these data suggest INXC
536 may be being expressed in neurons of the tentacles (single-cell RNA sequencing at a
537 greater depth of sequencing is needed to confirm). In addition to the tentacle bulb
538 expression, INXA is expressed in a small number of cells making up four distinct
539 domains in the floor of the aboral organ (Figure 4S, 4W). INXC is also expressed in
540 cells comprising 4 domains in the floor of the aboral organ (Figure 4G, 4W).

541

542 INXB and INXD are expressed in the tentacle bulbs, comb rows, pharynx, and aboral
543 organ (Figure 3 and 4). Like INXA and C, INXB is expressed in a small number of cells
544 comprising four distinct domains in the floor of the aboral organ (Figure 4T, 4X). INXD aboral
545 expression appears to form a ring in the aboral organ (Figure 4V, 4Z). INXB-D all exhibit a

546 speckled expression pattern in the pharynx (Figure 4D-F) and in the comb row region (Figure
547 4P-R).
548

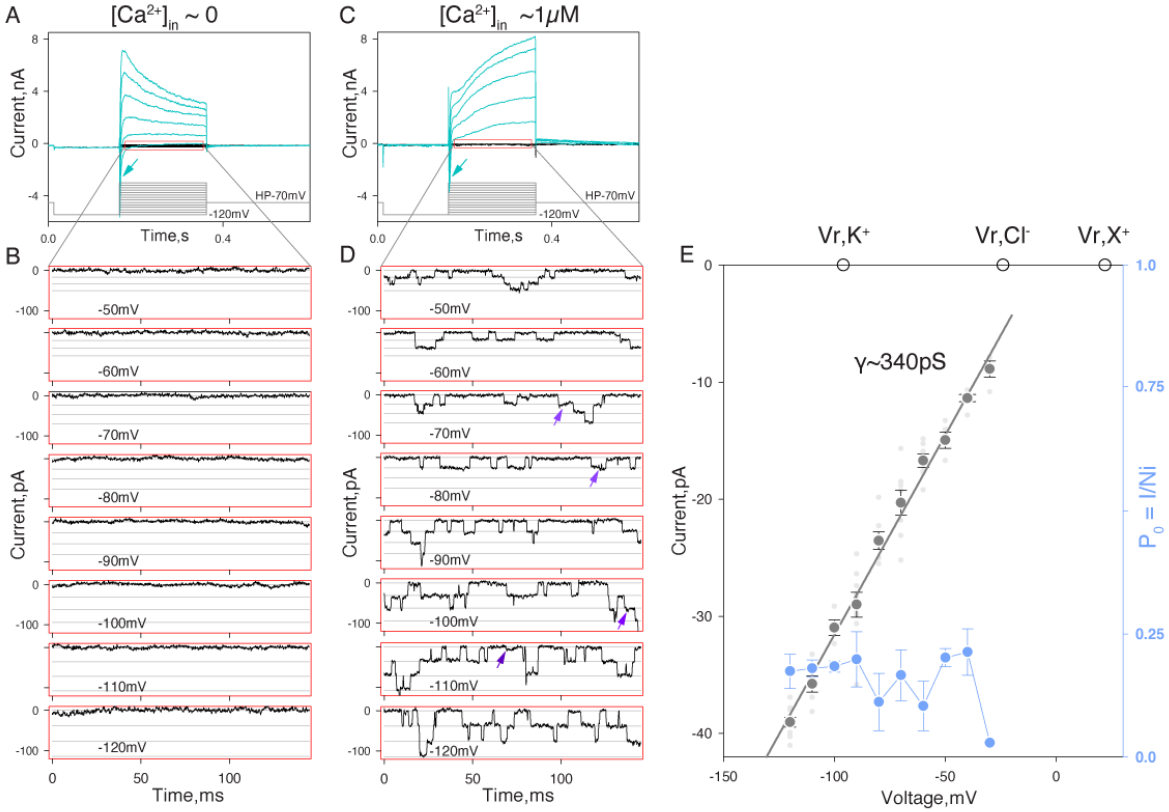


549 **Figure 5. Activity of putative innexons in *Mnemiopsis leidyi* muscle cells.**
550 Representative whole-cell currents recorded from isolated muscle cells in low (A,B) and high
551 (C,D) intracellular calcium. (A,C) Voltage protocol diagram showing muscle cells were initially
552 hyperpolarized by -50mV and then 200ms voltage steps were applied in 10mV increments.
553 Voltage gated currents are depicted in cyan (also Supplementary Figure 10 for details). For
554 example, inward currents characterized by fast activation/inactivation kinetics (arrows)
555 represent activity of voltage-gated sodium channels. Innexin channel activity outlined in red
556 represents traces without active voltage gated channels which are shown in more detail in B
557 and D. (B,D) Each panel displays portions of current traces obtained at different potentials (as

558 indicated). Horizontal lines depict unitary current levels. Arrows depict possible short-lived
559 subconductance states. Current values (y-axis) represent current values minus the basal
560 current level. (E) Plot of the relationship between current (pA) and voltage (mV) based on the
561 mean values (dark grey symbols) of single channel current amplitudes obtained at different
562 voltages (as in panel D). Data were obtained from 10 cells in total. Each light grey symbol
563 represents a single channel amplitude estimated for an individual cell. A linear approximation of
564 this relationship corresponds to a slope conductance of ~340 pS. Empty circles depict the
565 predicted reversal potentials of ideal potassium ($V_r$,$K^+$), chloride ($V_r$,$Cl^-$) and monovalent cation
566 ($V_r$,$X^+$) selective channels in the given experimental conditions. Note, unitary current-voltage
567 relationship suggests nonselective nature of the channel pore. Providing estimates of the
568 relative permeability of the channel for inorganic and organic ions would require further detailed
569 analysis. The blue symbols and lines (right y-axis) in panel D represent voltage dependence of
570 channel open probability expressed as $P_o$=I/Ni (where I = integral current, N = number of
571 channels detected in given conditions, i = single channel amplitude). Voltage dependence of $P_o$
572 was analyzed for 4 cells except for -30mV where n=1. Extracellular conditions in A and B are
573 identical. Data presented were filtered at 1 kHz and reduced 10-fold.
574
575
576 ***Electrophysiological evidence of innexin function in Mnemiopsis leidyi***
577
578 To begin to functionally characterize the ctenophore innexins, we tested whether
579 these channels, like their bilaterian counterparts (pannexins, innexins), are capable of
580 forming functional non-junctional channels (innexons). We tested whether the
581 conductance of channels in *M. leidyi* muscle cells was consistent with the single
582 channel-conductance parameters estimated for the innexon channels of other species

583 (250-550pS, in 150mM K+, Locovei et al. 2006; Bao et al. 2007; Kienitz et al. 2011).
584 We leveraged the high conductance of innexon channels to visualize activity of single
585 innexons (channel unitary currents) and characterize *the* channel gating.

586 We used isolated muscle cells because these are abundant in primary cell
587 cultures from oral lobe tissue and are easily identifiable both morphologically and
588 functionally. These cells contract upon excitation (Supplementary Movie 1), express
589 innexins ( Sebe-Pedros et al. 2018; Figure 5) as well as voltage-gated channels typical
590 for excitable cells (Sebe-Pedros et al. 2018; Figure 5A,C; Supplementary Figure10) and
591 are sensitive to amino acids such as glutamate/glycine (Alberstein et al. 2015;
592 Supplementary Figure 11 and Supplementary Movie 1).

593 We used whole-cell voltage clamp mode to record whole-cell currents and detect
594 potential activity of innexons. We focused exclusively on recording innexon unitary
595 currents. To better resolve innexon unitary currents in the whole-cell mode, only cells
596 characterized by relatively high input resistance (≥300MOhm) and cell-attached patch
597 seal resistance ≥1GOhm were chosen for analysis.

598 We tested for potential innexon channel activity in 0 intracellular $Ca^{2+}_{free}$ (1mM
599 EGTA +0 $Ca^{2+}$ added) condition using the experimental paradigm described in
600 methods. In 9 out of 9 cells chosen for analysis we found no indication of high
601 conductance channel activity (Fig5.A, B). These results suggest that *M. leidyi* innexon
602 channels require intracellular calcium for activation (e.g., Locovei et al. 2006; Bao et al.
603 2007).

604 We therefore tested whether these channels can be activated by relatively high
605 intracellular calcium (≥1μM). In 10 out of 24 cells examined, we were able to reliably

606 detect channel activity characterized by parameters potentially matching the following
607 basic properties of bilaterian innexin hemichannels: high single-channel conductance
608 (~340pS; Fig 5B-C), the apparent lack of ion selectivity (inferred reversal potential near
609 0; Fig 5C), the potential sensitivity to intracellular calcium, and the apparent lack of
610 voltage-dependent channel gating between -120 and -30mV (Fig 5E, blue line and
611 symbols, right Y-scale).
612

613 **DISCUSSION**

614

615 Our phylogenetic analyses suggest that innexins independently radiated within
616 Ctenophora. This pattern of lineage-specific diversification within major animal lineages
617 is an evolutionary tendency of innexins (Yen and Saier 2007) as it has also been
618 described in insects (Hasegawa and Turnbull 2014), tunicates, nematodes (Suzuki et
619 al. 2010), molluscs, annelids, and cnidarians (Fushiki et al. 2010; Abascal and Zardoya,
620 2013). This pattern of independent diversification in multiple animal lineages is unusual.
621 On the contrary, most gene superfamilies consist of a combination of early-established
622 families (i.e., families that arose in the stem ancestors of ancient lineages like Metazoa,
623 Parahoxozoa, and Bilateria) and more recently established families (i.e., those that
624 arose from lineage-specific expansions). Examples of this more common pattern of
625 expansion can be seen in homeoboxes (Ryan et al. 2006), Wnts (Pang et al. 2011),
626 LIM genes (Koch et al. 2012), trypsins (Babonis et al. 2019), opsins (Schnitzler et al.
627 2012), voltage-gated ion channels (Moran et al. 2015), and most other large
628 superfamilies. It is possible that this pattern of diversification in innexins is the

byproduct of processes that led to the establishment of major animal lineages. Alternatively, given that lineage-specific gene family expansion is often associated with adaptation and biological innovation (Lespinet et al 2002), it is possible that the diversification of innexins in the stem lineages of many major animal clades played a fundamental role in establishing these lineages

From analyses of public *M. leidyi* single-cell RNA-Seq data, we show that most cells express at least one innexin and more than 35% of cells express more than one innexin. This is similar to what is seen in other animals (e.g., *Caenorhabditis elegans* Altun et al. 2009; *Hydra vulgaris* Seibert et al. 2019) and suggests innexin channels have played a role in many cell types since the last common animal ancestor.

The identification of a cluster of innexins in the genomes of *M. leidyi*, *P. bachei* and *B. ovata* is a rare instance of such a conserved cluster of genes in ctenophores. As such, these data offer an example of how an extensive gene family arose via tandem duplication in ctenophores. In addition, when combined with expression data, the cluster provides a foundational example of genomic structure providing a functional role (i.e., gene regulation) in ctenophores. The expression data suggest that genes within the cluster are co-regulated in *M. leidyi*. INXB, INXC, and INXD have highly overlapping spatial patterns and are often expressed within the same cells. There is also single-cell evidence for overlapping expression between INXA and INXB, as well as INXA and INXD. These overlapping expression profiles suggest that there is regulatory architecture under purifying selection that is maintaining this cluster throughout long periods of evolutionary time. It is curious that the INXC expression overlaps with INXB and INXD, but that in all of the quantifiable expression experiments (i.e., single-embryo,

652 single-cell, and tissue RNA-Seq) INXC is expressed at a much lower level than INXB
653 and INXD.

654 The combined expression profiles of the highly expressed INXB and INXD
655 suggest that these genes are expressed in many cells, often in the same cell, and that
656 overall they are expressed in a consistent 2 to 1 ratio. The INXC gene expression
657 profile spatially overlaps with INXB and INXD, but the combined data point to this gene
658 being expressed at much lower levels than INXB and INXD. These expression data
659 combined with the extraordinary conserved nature of this gene cluster within
660 ctenophores, suggests a shared regulatory mechanism and presents the best such
661 foothold from which to interrogate gene regulation from within ctenophores. We
662 hypothesize that the coordinated expression of these innexin genes has some bearing
663 on the subunit makeup of the resulting channels and potential gap junctions. Given that
664 the cluster has been maintained over millions of years, we further hypothesize that a
665 similar regulatory system and subunit makeup was present in the last common ancestor
666 of all ctenophores (at least in the last common ancestor of the four ctenophores we
667 analyzed).

668 Our in situ gene expression data suggests that innexins are expressed in
669 adjacent domains of the aboral organ (Figure 4W–Z). It is difficult to discern from these
670 data whether the comb row expression of INXB–D involves comb plate cilia, gametes,
671 photocytes or other cell types located in this region. In published single-cell RNA-Seq
672 data (Sebe-Pedros et al. 2018), INXB and INXD are considered marker genes for
673 clusters of cells (metacells) labeled as epithelial, digestive, and muscle cells (Figure

3D), but INXB and INXD are also highly expressed in many other cells including several metacells that were not labeled in the original study (Figure 3E).

While significant progress has been made characterizing the functional, electrophysiological properties of gap junction channels in bilaterians (e.g. Wang et al. 2014; Bhattacharya et al. 2019; Walker and Schafer 2020; for review Dahl and Muller 2014; Skerrett and Williams 2017 and Guiza et al. 2018) relatively little is known about gap junction channels in non-bilaterian lineages. Here we provide the first demonstration of the activity of putative innexon channels from ctenophore muscle cells. The smooth muscle cells of *M. leidyi* are excellent cells to investigate innexins: there is published ultrastructural evidence of gap junctions connecting these cells (Hernandez-Nicaise et al. 1984), most smooth muscles sampled in published RNA-Seq data express INXB (87 of 186 cells) and INXD (78 of 186 cells), and the electrophysiological and molecular properties can be studied in great detail due to the ability to maintain these cells in primary cell culture (Supplementary Figure 10).

Potential effects of intracellular calcium ions on gap junctional channels are likely more complex than were initially suggested (e.g., Deleze and Loewenstein 1976; Loewenstein and Rose 1978; reviewed by Skerrett and Williams 2017) and not limited to suppression of electrical and/or dye coupling by elevated cytoplasmic calcium. Indeed, activation by intracellular calcium in physiologically relevant concentration range appears to be an important common property of non-junctional pannexins and innexins (Locovei et al. 2006; Bao et al. 2007; Kienitz et al. 2011; Dahl and Muller 2014).

Our results outline the following basic physiological properties of *M. leidyi* innexin channels: (1) high single-channel conductance, (2) the presence of subconductance states, (3) the apparent lack of ion selectivity, (4) the potential sensitivity to intracellular calcium, and (5) the apparent lack of voltage dependency of channel gating (at least between -120 to -30 mV).

While individually, these properties could be attributed to other channel types, collectively, they are consistent with properties of gap junction channels. For example, Maxi-Cl channels (SLCO2A1, a member of the solute carrier organic anion transporter family) are expressed in ctenophore muscle cells (e.g. ML18358a is expressed in 22% of a metacell identified as muscle–c43–in Sebe-Pedros et al. 2018) and would also be characterized by high unitary conductance, the occurrence of subconductance states, and calcium dependent activity, but these channels are anion-selective and exhibit a distinct voltage dependence of their open probability (Sabirov et al. 2017). Similarly, we can eliminate the potential involvement of large conductance calcium-activated potassium channels (ML128229a is expressed in 47% of a muscle metacell–c47) because of the ion selectivity of these channels. We can also eliminate inositol 1,4,5-trisphosphate receptor (insP3R) channels (ML25824a shows no expression in muscle metacells above background) since these are calcium sensitive, nonselective cation channels, require cytoplasmic IP3 to be active, and otherwise show extremely low basal activity (Dellis et al. 2006). Furthermore, the relatively high concentration of divalent cations used in our experiments would dramatically decrease unitary conductance in InsP3R channels (Bezprozvanny and Ehrlich 1994; Mak and Foskett 1998). Thus we

718 conclude that the properties of the channels we characterize here, collectively, are
719 consistent with those of innexons.

720 To more rigorously implicate the innexins in the ctenophore intercellular
721 signaling, future efforts will require exploring the detailed functional properties and
722 pharmacological and molecular profiles of signaling pathways involved. Our
723 electrophysiological results will have a substantial impact on orienting future efforts to
724 uncover the role of innexins in distributing signals throughout ctenophore neuro-
725 muscular and neuro-sensory networks.

726

727 **CONCLUSION:**

728

729 Our data show that *M. leidyi* innexins are expressed widely and some at very
730 high levels in almost every cell type. This is consistent with ultrastructural studies
731 (Satterlie and Case, 1978; Hernandez-Nicaise and Amsellem, 1980; Hernandez-
732 Nicaise et al. 1984; Anctil, 1985) showing that, like in other animals (e.g. Hall, 2017),
733 gap junctions are broadly deployed throughout the ctenophore body plan. Our whole-
734 cell recordings of *M. leidyi* smooth muscle cells show channel activity consistent with
735 the channel activity of gap junction channels in bilaterians. The genomic clustering of
736 innexins suggests an ancient regulatory mechanism underlying innexin expression.
737 Together these data support a key role for innexins and gap junctions in the biology of
738 ctenophores and provide an essential starting point for future exploration of innexins,
739 genome regulation, and gap junctions in ctenophores.

740

741

742 **ACKNOWLEDGEMENTS**

743

744 We thank Michel Anctil for helpful conversations. We thank David Ortiz for help
745 generating Figure 3. We thank Barry Ache for a critical reading of parts of this
746 manuscript. We thank James Strother for access to equipment and conversations. The
747 views expressed in this manuscript do not necessarily reflect the views of those
748 acknowledged.

749 This work was supported by the National Science Foundation (DEB-1542597 to
750 J.F.R.) and the National Science Foundation Research Experience for Undergraduates
751 (REU) Program (DBI-1156528 to J.F.R.). This research was supported by an Allen
752 Distinguished Investigator Award, a Paul G. Allen Frontiers Group advised grant of the
753 Paul G. Allen Family Foundation to J.F.R. and M.Q.M. A.E. was supported by a
754 National Science Foundation Postdoctoral Research Fellowship in Biology (DBI-
755 2010755). The funders had no role in study design, data collection and analysis,
756 decision to publish, or preparation of the manuscript.

757
758
759

760 **References**
761
762 Abascal F, Zardoya R. Evolutionary analyses of gap junction protein families. *Biochim*
763 *Biophys Acta*. 2013 1828:4-14.

764 Abascal F, Zardoya R. LRRC8 proteins share a common ancestor with pannexins, and
765 may form hexameric channels involved in cell-cell communication. *Bioessays*. 2012
766 34:551-560.

767 Alberstein R, Grey R, Zimmet A, Simmons DK, Mayer ML. 2015. Glycine activated ion
768 channel subunits encoded by ctenophore glutamate receptor genes. Proc Natl Acad Sci
769 U S A 112:E6048-6057.

770 Altun ZF, Chen B, Wang ZW, Hall DH. High resolution map of *Caenorhabditis elegans*
771 gap junction proteins. *Developmental Dynamics: An official publication of the American*
772 *Association of Anatomists*. 2009 238(8):1936-50.

773 Anctil M. Cholinergic and Monoaminergic Mechanisms Associated with Control of
774 Bioluminescence in the Ctenophore *Mnemiopsis leidyi*. *Journal of Experimental*
775 *Biology*. 1985 119:225-238.

776 Babonis LS, DeBiasse MB, Francis WR, Christianson LM, Moss AG, Haddock SHD,
777 Martindale MQ, Ryan JF. Integrating Embryonic Development and Evolutionary History
778 to Characterize Tentacle-Specific Cell Types in a Ctenophore. *Molecular Biology and*
779 *Evolution*. 2018 35:2940-2956.

780 Babonis LS, Ryan JF, Enjolras C, Martindale MQ. Genomic analysis of the tryptome
781 reveals molecular mechanisms of gland cell evolution. *EvoDevo*. 2019 10(1):1-18.

782 Bao L, Samuels S, Locovei S, Macagno ER, Muller KJ, Dahl G. Innexins form two types
783 of channels. *Febs Letters*. 2007 581:5703-5708.

784 Bezprozvanny I, Ehrlich BE. Inositol (1,4,5)-Trisphosphate (Insp(3))-Gated Ca
785 Channels from Cerebellum - Conduction Properties for Divalent-Cations and Regulation
786 by Intraluminal Calcium. *Journal of General Physiology*. 1994 104:821-856.

787 Bhattacharya A, Aghayeva U, Berghoff EG, Hobert O. 2019. Plasticity of the Electrical
788 Connectome of C. elegans. Cell 176:1174-+.

789 Bobkov YV, Corey EA, Ache BW. The pore properties of human nociceptor channel
790 TRPA1 evaluated in single channel recordings. *Biochimica et Biophysica Acta (BBA)-*
791 *Biomembranes*. 2011 1808(4):1120-8.

792 Bruzzone R, White TW, Paul DL. Connections with connexins: The molecular basis of
793 direct intercellular signaling. *European Journal of Biochemistry*. 1996 238:1-27.

794 Dahl G, Muller KJ. Innexin and pannexin channels and their signaling. *Febs Letters*.
795 2014 588:1396-1402.

796 DeBiasse MB, Ryan JF. Phylotocol: Promoting Transparency and Overcoming Bias in
797 Phylogenetics. *Systematic Biology*. 2019 68:672-678.

798 Deleze J, Loewenstein WR. Permeability of a cell junction during intracellular injection
799 of divalent cations. *The Journal of Membrane Biology*. 1976. 28:71-86.

800 Dellis O, Dedos SG, Tovey SC, Taufiq-Ur-Rahman, Dubel SJ, Taylor CW. Ca2+ entry
801 through plasma membrane IP3 receptors. *Science*. 2006 313:229-233.

802 Dunn CW, Hejnol A, Matus DQ, Pang K, Browne WE, Smith SA, Seaver E, Rouse GW,
803 Obst M, Edgecombe GD, et al. Broad phylogenomic sampling improves resolution of
804 the animal tree of life. *Nature*. 2008 452:745-U745.

805 Dunn CW, Leys SP, Haddock SHD. The hidden biology of sponges and ctenophores.
806 *Trends in Ecology & Evolution*. 2015 30:282-291.

807 Finn RD, Clements J, Eddy SR. HMMER web server: interactive sequence similarity
808 searching. *Nucleic Acids Research*. 2011 39:W29-W37.

809 Fushiki D, Hamada Y, Yoshimura R, Endo Y. Phylogenetic and bioinformatic analysis of
810 gap junction-related proteins, innexins, pannexins and connexins. *Biomedical*
811 *Research*. 2010 31:133-142.

812 Goodenough DA, Paul DL. Gap Junctions. *Cold Spring Harbor Perspectives in Biology*.
813 2009 1.

814 Guiza J, Barria I, Saez JC, Vega JL. Innexins: Expression, Regulation, and Functions.
815 *Frontiers in Physiology*. 2018 9.

816 Hall DH. Gap Junctions in C-elegans: Their Roles in Behavior and Development.
817 *Developmental Neurobiology*. 2017 77:587-596.

818 Hasegawa DK, Turnbull MW. Recent findings in evolution and function of insect
819 innexins. *Febs Letters*. 2014 588:1403-1410.

820 Hernandez AM, Ryan JF. Horizontally transferred genes in the ctenophore *Mnemiopsis*
821 *leidyi*. *PeerJ*. 2018 6.

822 Hernandez-Nicaise ML, Amsellem J. Ultrastructure of the Giant Smooth-Muscle Fiber of
823 the Ctenophore *Beroe ovata*. *Journal of Ultrastructure Research*. 1980 72:151-168.

824 Hernandez-Nicaise ML, Nicaise G, Malaval L. Giant Smooth-Muscle Fibers of the
825 Ctenophore *Mnemiopsis leidyi* - Ultrastructural-Study of Insitu and Isolated Cells. 1984
826 *Biological Bulletin* 167:210-228.

827 Hernandez-Nicaise ML, Nicase G, & Reese TS. Intercellular junctions in ctenophore
828 integument. In: Evolution of the First Nervous Systems. Aanderson PAV, editor. New
829 York: Plenum Press. 1989 p. 21–32.

830 Horridge GA. Recent studies on the Ctenophora. In: Coelenterate Biology: Reviews and
831 New Perspectives, Muscatine L and Lenhoff HM editors, New York: Academic Press.
832 1974 p. 439-468.

833 Jager M, Chiori R, Alie A, Dayraud C, Queinnec E, Manuel M. New Insights on
834 Ctenophore Neural Anatomy: Immunofluorescence Study in *Pleurobrachia pileus*
835 (Muller, 1776). *Journal of Experimental Zoology Part B-Molecular and Developmental*
836 *Evolution*. 2011 316b:171-187.

837 Kanaporis G, Brink PR, Valiunas V. Gap junction permeability: selectivity for anionic
838 and cationic probes. *American Journal of Physiology-Cell Physiology*. 2011 300:C600-
839 C609.

840 Katoh K, Toh H. Recent developments in the MAFFT multiple sequence alignment
841 program. *Briefings in Bioinformatics*. 2008 9:286-298.

842 Kienitz MC, Bender K, Dermietzel R, Pott L, Zoidl G. Pannexin 1 constitutes the large
843 conductance cation channel of cardiac myocytes. *Journal of Biological Chemistry*. 2011
844 286:290-298.

845 Kinsella RJ, Kahari A, Haider S, Zamora J, Proctor G, Spudich G, Almeida-King J,
846 Staines D, Derwent P, Kerhornou A, et al. Ensembl BioMarts: a hub for data retrieval
847 across taxonomic space. *Database*. 2011 2011-bar030.

848 Koch BJ, Ryan JF, Baxevanis AD. The Diversification of the LIM Superclass at the
849 Base of the Metazoa Increased Subcellular Complexity and Promoted Multicellular
850 Specialization. *Plos One*. 2012 7.

851 Koval M, Molina SA, Burt JM. Mix and match: Investigating heteromeric and heterotypic
852 gap junction channels in model systems and native tissues. *Febs Letters.* 2014
853 588:1193-1204.

854 Lespinet O, Wolf YI, Koonin EV, Aravind L. The role of lineage-specific gene family
855 expansion in the evolution of eukaryotes. *Genome Research*. 2002 12(7):1048-59.

856 Levin M, Anavy L, Cole AG, Winter E, Mostov N, Khair S, Senderovich N, Kovalev E,
857 Silver DH, Feder M, et al. The mid-developmental transition and the evolution of animal
858 body plans. 2016 *Nature* 531:637-+.

859 Leys SP. Elements of a 'nervous system' in sponges. *Journal of Experimental Biology*.
860 2015 218:581-591.

861 Li B, Dewey CN. RSEM: accurate transcript quantification from RNA-Seq data with or
862 without a reference genome. *BMC Bioinformatics*. 2011 1:1-6.

863 Linden J, Koch-Nolte F, Dahl G. Purine Release, Metabolism, and Signaling in the
864 Inflammatory Response. *Annual Review of Immunology*. 2019 Vol 37, 2019 37:325-
865 347.

866 Locovei S, Wang JJ, Dahl G. Activation of pannexin 1 channels by ATP through P2Y
867 receptors and by cytoplasmic calcium. *Febs Letters.* 2006 580:239-244.

868 Loewenstein WR. Permeability of Membrane Junctions. *Annals of the New York*
869 *Academy of Sciences*. 1966 137:441-472.

870 Loewenstein WR, Rose B. Calcium in (junctional) intercellular communication and a
871 thought on its behavior in intracellular communication. *Annals of the New York*
872 *Academy of Sciences.* 1978 307:285-307.

873 Love MI, Huber W, Anders S. Moderated estimation of fold change and dispersion for
874 RNA-seq data with DESeq2. *Genome Biology*. 2014 15.

875 Mak DOD, Foskett JK. Effects of divalent cations on single-channel conduction
876 properties of *Xenopus* IP3 receptor. *American Journal of Physiology-Cell Physiology*.
877 1998 275:C179-C188.

878 Mitchell DG, Edgar A, Martindale MQ. Improved histological fixation of gelatinous
879 marine invertebrates. *Frontiers in Zoology*. 2021 Dec;18(1):1-3.

880 Moran Y, Barzilai MG, Liebeskind BJ, Zakon HH. Evolution of voltage-gated ion
881 channels at the emergence of Metazoa. *Journal of Experimental Biology*. 2015
882 218:515-525.

883 Moreland RT, Nguyen AD, Ryan JF, Baxevanis AD. The *Mnemiopsis* Genome Project
884 Portal: integrating new gene expression resources and improving data visualization.
885 *Database*. 2020 2020-baaa029.

886 Moroz LL, Kocot KM, Citarella MR, Dosung S, Norekian TP, Povolotskaya IS,
887 Grigorenko AP, Dailey C, Berezikov E, Buckley KM, et al. The ctenophore genome and
888 the evolutionary origins of neural systems. *Nature*. 2014 510:109-+.

889 Moroz LL, Kohn AB. Independent origins of neurons and synapses: insights from
890 ctenophores. Philosophical Transactions of the Royal Society B: Biological Sciences.
891 2016 Jan 5;371(1685):20150041.

892 Oshima A, Matsuzawa T, Nishikawa K, Fujiyoshi Y. Oligomeric Structure and
893 Functional Characterization of *Caenorhabditis elegans* Innexin-6 Gap Junction Protein.
894 *Journal of Biological Chemistry*. 2013 288:10513-10521.

895 Oshima A, Matsuzawa T, Murata K, Tani K, Fujiyoshi Y. Hexadecameric structure of an
896 invertebrate gap junction channel. *Journal of Molecular Biology*. 2016 428:1227-1236.

897 Pang K, Martindale MQ. Developmental expression of homeobox genes in the
898 ctenophore *Mnemiopsis leidyi*. *Development Genes and Evolution*. 2008 218:307-319.

899 Pang K, Ryan JF, Baxevanis AD, Martindale MQ. Evolution of the TGF-beta signaling
900 pathway and its potential role in the ctenophore, *Mnemiopsis leidyi*. *Plos One*. 2011

6:e24152.

Phelan P, Bacon JP, Davies JA, Stebbings LA, Todman MG, Avery L, Baines RA, Barnes TM, Ford C, Hekimi S, Lee R. Innexins: a family of invertebrate gap-junction proteins. Trends in genetics: TIG. 1998 Sep;14(9):348.

Phelan P, Starich TA. Innexins get into the gap. *Bioessays*. 2001 23:388-396.

Ronquist F, Huelsenbeck JP. MrBayes 3: Bayesian phylogenetic inference under mixed models. *Bioinformatics*. 2003 19:1572-1574.

Ryan JF, Burton PM, Mazza ME, Kwong GK, Mullikin JC, Finnerty JR. The cnidarian-bilaterian ancestor possessed at least 56 homeoboxes: evidence from the starlet sea anemone, Nematostella vectensis. *Genome Biology*. 2006 7:R64.

Ryan JF, Pang K, Schnitzler CE, Nguyen AD, Moreland RT, Simmons DK, Koch BJ, Francis WR, Havlak P, Smith SA, et al. The Genome of the Ctenophore *Mnemiopsis leidyi* and Its Implications for Cell Type Evolution. *Science*. 2013 342:1336-+.

Sabirov RZ, Merzlyak PG, Okada T, Islam MR, Uramoto H, Mori T, Makino Y, Matsuura H, Xie Y, Okada Y. The organic anion transporter SLCO2A1 constitutes the core component of the Maxi-Cl channel. *Embo Journal*. 2017 36:3309-3324.

Sachkova MY, Nordmann EL, Soto-Angel JJ, Meeda Y, Gorski B, Naumann B, Dondorp D, Chatzigeorgiou M, Kittelmann M, Burkhardt P. Neuropeptide repertoire and 3D anatomy of the ctenophore nervous system. *Current Biology*. 2021 31:5274-5285 e5276.

Sasson DA, Ryan JF. The sex lives of ctenophores: the influence of light, body size, and self-fertilization on the reproductive output of the sea walnut, *Mnemiopsis leidyi*. *PeerJ*. 2016 4.

Satterlie, Richard A. "The search for ancestral nervous systems: an integrative and comparative approach." *Journal of Experimental Biology* 218.4 (2015): 612-617.

Satterlie RA, Case JF. Gap Junctions Suggest Epithelial Conduction within Comb Plates of Ctenophore *Pleurobrachia bachei*. *Cell and Tissue Research*. 1978 193:87-91.

Schnitzler CE, Pang K, Powers ML, Reitzel AM, Ryan JF, Simmons D, Tada T, Park M, Gupta J, Brooks SY, et al. Genomic organization, evolution, and expression of photoprotein and opsin genes in *Mnemiopsis leidyi*: a new view of ctenophore photocytes. *BMC Biology.* 2012 10.

Schultz DT, Francis WR, McBroome JD, Christianson LM, Haddock SH, Green RE. A chromosome-scale genome assembly and karyotype of the ctenophore *Hormiphora californensis*. *G3*. 2021 11:jkab302.

936 Sebe-Pedros A, Chomsky E, Pang K, Lara-Astiaso D, Gaiti F, Mukamel Z, Amit I,
937 Hejnol A, Degnan BM, Tanay A. Early metazoan cell type diversity and the evolution of
938 multicellular gene regulation. *Nature Ecology & Evolution*. 2018 2:1176-+.

939 Senatore A, Reese TS, Smith CL. Neuropeptidergic integration of behavior in
940 *Trichoplax adhaerens*, an animal without synapses. *Journal of Experimental Biology*.
941 2017 220:3381-3390.

942 Siebert S, Farrell JA, Cazet JF, Abeykoon Y, Primack AS, Schnitzler CE, Juliano CE.
943 Stem cell differentiation trajectories in *Hydra* resolved at single-cell resolution. *Science*.
944 2019 26;365(6451):eaav9314.

945 Skerrett IM, Williams JB. A structural and functional comparison of gap junction
946 channels composed of connexins and innexins. *Developmental Neurobiology*. 2017
947 77:522-547.

948 Slivko-Koltchik G, Kuzentzov V, and Panchin Y. Evolution of Pannexin/Innexin Gap
949 Junction Protein Family. Information Technology and Systems. The 40th
950 Interdisciplinary Conference & School; St Petersburg, Russia. 2016 p. 151-154.

951 Slivko-Koltchik GA, Kuznetsov VP, Panchin YV. Are there gap junctions without
952 connexins or pannexins? *BMC Evolutionary Biology*. 2019 19.

953 Suzuki TG, Ogino K, Tsuneki K, Furuya H. Phylogenetic analysis of dicyemid
954 mesozoans (phylum Dicyemida) from innexin amino acid sequences: dicyemids are not
955 related to Platyhelminthes. *Journal of Parasitology*. 2010 96:614-625.

956 Tamm SL. Ctenophora. In: Electrical Conduction and Behaviour in 'Simple'
957 Invertebrates. Shelton GAB, ed., 1982 p. 266–358. Clarendon Press, Oxford, UK.

958 Tamm SL. Mechanical Synchronization of Ciliary Beating within Comb Plates of
959 Ctenophores. *Journal of Experimental Biology*. 1984 113:401-&.

960 Tamm SL. Cilia and the life of ctenophores. *Invertebrate Biology*. 2014 133:1-46.

961 Walker DS, Schafer WR. Distinct roles for innexin gap junctions and hemichannels in
962 mechanosensation. *eLife* 2020 9.

963 Wang JJ, Ambrosi C, Qiu F, Jackson DG, Sosinsky G, Dahl G. The membrane protein
964 Pannexin1 forms two open-channel conformations depending on the mode of
965 activation. *Science Signaling*. 2014 7.

966 Welzel G, Schuster S. Connexins evolved after early chordates lost innexin diversity.
967 *eLife* 2022 11:e74422.

968 Yeager M, Harris AL. Gap junction channel structure in the early 21st century: facts and
969 fantasies. Current opinion in cell biology. 2007 Oct 1;19(5):521-8.

970 Yen MR, Saier MH. Gap junctional proteins of animals: The innexin/pannexin
971 superfamily. *Progress in Biophysics & Molecular Biology*. 2007 94:5-14.

972 Zhou X, Shen XX, Hittinger CT, Rokas A. Evaluating fast maximum likelihood-based
973 phylogenetic programs using empirical phylogenomic data sets. Molecular biology and
974 evolution. 2018 Feb 1;35(2):486-503.